



HAL
open science

Spectral analysis of the Martian atmospheric turbulence: InSight observations

Orkun Temel, Cem Senel, Aymeric Spiga, Naomi Murdoch, Don Banfield,
Ozgur Karatekin

► **To cite this version:**

Orkun Temel, Cem Senel, Aymeric Spiga, Naomi Murdoch, Don Banfield, et al.. Spectral analysis of the Martian atmospheric turbulence: InSight observations. 2022. hal-03670716

HAL Id: hal-03670716

<https://hal.science/hal-03670716>

Preprint submitted on 17 May 2022

HAL is a multi-disciplinary open access archive for the deposit and dissemination of scientific research documents, whether they are published or not. The documents may come from teaching and research institutions in France or abroad, or from public or private research centers.

L'archive ouverte pluridisciplinaire **HAL**, est destinée au dépôt et à la diffusion de documents scientifiques de niveau recherche, publiés ou non, émanant des établissements d'enseignement et de recherche français ou étrangers, des laboratoires publics ou privés.

Spectral analysis of the Martian atmospheric turbulence: InSight observations

Orkun Temel^{1,2}, Cem Berk Senel², Aymeric Spiga^{3,4}, Naomi Murdoch⁵, Don
Banfield⁶ and Ozgur Karatekin²

¹KU Leuven, Institute of Astronomy, Leuven, Belgium

²Royal Observatory of Belgium, Reference Systems and Planetology, Brussels, Belgium

³Laboratoire de Météorologie Dynamique/Institut Pierre Simon Laplace (LMD/IPSL), Sorbonne
Université, Centre National de la Recherche Scientifique (CNRS), École Polytechnique, École Normale
Supérieure (ENS), Paris, France

⁴Institut Universitaire de France, Paris, France

⁵Institut Supérieur de l'Aéronautique et de l'Espace (ISAE-SUPAERO), Université de Toulouse, Toulouse,
France

⁶Cornell University, New York, U.S.A

Key Points:

- We make use of in-situ observations to investigate the Martian atmospheric turbulence.
- We find distinct spectral behaviours of turbulence for daytime and night-time conditions.
- We report important effects of a regional dust storm and gravity wave activity on the turbulence energy cascade.

Corresponding author: Orkun Temel, orkun.temel@oma.be

Abstract

In this study, we perform a detailed spectral analysis of the turbulent energy cascade using the in-situ observations by NASA's InSight lander on Mars. A recent study on the daytime Martian boundary layer using the InSight observations showed that the conventional Kolmogorov energy cascade of inertial sub-range fails to predict the spectral density of pressure (Banfield et al., 2020). Here we extend this by investigating diurnal and seasonal variations in the spectral density of pressure, as the indicator of the Martian atmospheric turbulence. We show distinct spectral behaviours for the daytime and nighttime conditions. Moreover, we report the important effects of regional dust storms, gravity waves, bore and solitary waves on the turbulent energy cascade. Our results show that the presence of a dust storm and gravity wave activity can enhance the turbulence of the nighttime boundary layer of Mars despite the extreme stably stratified conditions compared to the terrestrial case.

Plain Language Summary

Turbulent mixing in the first kilometers above the planetary surface, the atmospheric boundary layer, drives the transport of momentum, heat and volatiles between a planet's surface and its atmosphere. Thus, it requires a detailed investigation by observations to be able to understand better the atmospheric dynamics, and most importantly, the processes controlling them. In this study, we make use of the InSight lander's pressure observations to understand how the Martian atmospheric turbulence differs over a daily cycle and in different seasons. Here we showed that the nocturnal near-surface environment of Mars can be more turbulent than thought before and it can have important implications for the Martian atmospheric seasonal cycles. We also find that the daytime and nocturnal turbulence exhibits different behaviours, which are affected by the presence of a regional dust storm and gravity wave activity.

1 Introduction

NASA's InSight (Interior exploration using Seismic Investigations, Geodesy and Heat Transport) mission landed in Elysium Planitia, a flat-smooth plain just north of the equator on Mars, on Mars year (MY) 34, after the Northern hemisphere Winter Solstice, $L_s = 295.5$ (26 November 2018) (Banerdt et al., 2020). In addition to the interior structure, composition and thermal state of Mars, the InSight mission is devoted to a better understanding of near-surface atmospheric conditions (Spiga et al., 2018; Banfield et al., 2020; Spiga et al., 2020), which are notably driven by the turbulent transport in the planetary boundary layer (PBL).

The Martian PBL is one important component of the Martian atmosphere, affecting the amount of dust lifted from its surface and altering the atmospheric dust cycle (Toigo et al., 2003), which leads to inter-annual and seasonal variations in the surface meteorological conditions (Montabone et al., 2015; Senel et al., 2021). Therefore, studying the Martian PBL is important to improve our understanding of the Martian climate. However, our current understanding of the Martian PBL mainly depends on the near-surface observations by previous landers (Hess et al., 1977; Schofield et al., 1997; Taylor et al., 2008; Martínez et al., 2009; Viúdez-Moreiras et al., 2019), which lacked either the accuracy, the continuity, or the high-frequency in-situ observations necessary to understand the turbulent energy cascade. Among the previous landers, only Viking (Hess et al., 1977; Chamberlain et al., 1976), Pathfinder (Schofield et al., 1997; Seiff et al., 1997), Phoenix (Holstein-Rathlou et al., 2010) and Mars Science Laboratory (MSL) (Gómez-Elvira et al., 2012; Viúdez-Moreiras et al., 2019) provided in-situ meteorological data. However, their sampling frequency was limited up to 1, 0.25, 0.5 and 1 Hz, respectively. Unlike previous landers, the InSight lander can detect turbulent fluctuations continuously up to a pressure sampling frequency of 10 Hz (Spiga et al., 2018; Banfield et al., 2019). Moreover, the long temporal coverage of InSight allows us to investigate seasonal variations caused by the Martian dust cycle using a continuous high-resolution observational dataset. Here, we make use of atmospheric pressure

71 observations of InSight, obtained with at high frequency, making the analysis of the transfer
 72 of energy between large and small scale turbulent structures (eddies), in other words the
 73 energy cascade. Banfield et al. (2020) demonstrated that the slope in the energy spectrum
 74 of daytime pressure measured by InSight in the turbulent range is similar to Earth's and
 75 similarly at odds with theoretical expectations. This deserves further examination of the
 76 InSight data, including both nocturnal and daytime turbulence.

77 In this paper, we perform a spectral analysis on the high-resolution pressure observa-
 78 tions acquired by the InSight lander. We focus on three main research questions: (1) How
 79 do the diurnal variations affect the spectral dynamics of turbulence on Mars? (2) What is
 80 the effect of atmospheric dust content? (3) Does gravity wave activity play an important
 81 role on the observed spectral slopes? We compute the turbulence spectrum for daytime and
 82 nocturnal (for two different local hour intervals, called as evening and nighttime) conditions.
 83 The turbulence spectrum shows the variation of the energy content for different frequency
 84 bands, which correspond to different turbulent length scales. For the spectral analysis of
 85 turbulence, Kolmogorov energy cascade is widely used to understand the dynamics between
 86 large and small scales, showing a spectral slope of $-7/3$ for pressure fluctuations (Tsuji &
 87 Ishihara, 2003). Despite the fact that the validity of Kolmogorov's energy cascade is also
 88 disputed for terrestrial boundary layers (Albertson et al., 1998), it is still used as a baseline
 89 for spectral analysis studies for turbulent boundary layers (Tsuji et al., 2007; Kunkel &
 90 Marusic, 2006).

91 2 Data and methodology

92 We make use of the data from InSight's pressure sensor, which performed observations
 93 up to a sampling frequency of 10 Hz after sol 168 and 2 Hz before sol 168, with noise levels
 94 of $10 \text{ mPa Hz}^{-0.5}$ and $50 \text{ mPa Hz}^{-0.5}$ between a range of from 0.1 Hz to 1 Hz, and at 0.01
 95 Hz, respectively (Banfield et al., 2019). These sampling frequencies correspond to Nyquist
 96 frequencies ($f_{Nyq} = 0.5f_s$) of 5 Hz and 1 Hz.

97 The sols on which we perform the spectral analysis are chosen based on the initial
 98 atmospheric results of the InSight lander (Banfield et al., 2020). First, we search for a
 99 sol without a regional dust storm and gravity wave activity to be able to make distinction
 100 between the spectral behaviours of daytime and nighttime conditions, solely based on diurnal
 101 variations. Therefore, to investigate (1), we choose a sol without a regional dust storm (sol 18
 102 after the landing). The difference in the spectral behaviour of turbulence between daytime
 103 and nocturnal is related to the turbulent coherent structures. For (2), we focus on three
 104 sols before and during a regional dust storm (sols 18, 46 and 55). For (3), we investigate the
 105 sols with and without gravity wave activity. For our observational analysis we use a time
 106 window of 5 hours for daytime, evening and nighttime conditions (corresponding to 11-16,
 107 18-23 and 00-05 LMST).

108 We perform the spectral analysis using the Fourier transform from time to frequency
 109 domain. Suppose that a fluctuation series of pressure in the time domain is $p'(t)$. Then the
 110 series of turbulence fluctuations under consideration can be transformed from time, t , to
 111 frequency domain, ω , in order to possess the distribution of turbulent energy content over
 112 a wide range of eddy scales. Regarding this transform, the complex Fourier transform (also
 113 the fast Fourier transform - FFT algorithm) can be applied in the time domain to compute
 114 the turbulence spectrum in the frequency domain, $E_{pp}(\omega)$, as follows:

$$E_{pp}(\omega) = \frac{2}{\pi} \int_0^{\infty} p'p'(t)e^{-i\omega t} dt \quad (1)$$

115 where $p'(t)$ is the pressure fluctuations in the time domain and $E_{pp}(\omega)$ refers to the turbulent
 116 pressure spectra along with a wide range of frequency. By formulating the turbulence spectra
 117 as a function of frequency, large-scale eddies are represented in the lower frequency bands
 118 and the smaller eddies fall to the high frequency zone.

119 Before using our spectral analysis methodology, we first perform a verification study
 120 by comparing our calculated spectral slope for daytime conditions with the one obtained by
 121 (Banfield et al., 2020). As presented in Fig. S1, we find a spectral slope of $-5/3 \approx -1.7$,
 122 consistent with the previously published result.

123 3 Diurnal variations of turbulence as observed by the InSight lander

124 First, we investigate how the spectral behaviour of turbulence varies during a sol,
 125 when neither a regional dust storm nor gravity wave activity is present. Hence, we can
 126 interpret the differences we find in the observations solely as a result of diurnal variations
 127 in the radiative surface forcing. During the daytime conditions, the turbulent mixing in
 128 the boundary layer is enhanced as a result of surface heating, leading to strong vertical
 129 transport of momentum and heat, and forming larger convective structures (Kaimal et al.,
 130 1976; Schmidt & Schumann, 1989; Spiga et al., 2010, 2016; Senel et al., 2019, 2020; Temel
 131 et al., 2021). However, during the nocturnal conditions, convective turbulence is suppressed
 132 with the negative buoyancy flux, resulting from the surface cooling rate. Therefore, the
 133 scale of coherent structures in the stably stratified Martian PBL (hereafter SBL) is much
 134 smaller compared to the daytime PBL, similar to the terrestrial case (Mason & Derbyshire,
 135 1990; Mayor, 2017).

136 As suggested by Banfield et al. (2020), the Martian SBL is exposed to intermittent
 137 turbulence, the irregular alteration of turbulence, similar to Earth's SBL. The difference
 138 between the terrestrial SBL and the Martian SBL is that the latter exhibits more intermit-
 139 tency due to its lower atmospheric density. Despite these similarities between the terrestrial
 140 and the Martian boundary layers, the Martian PBL can be regarded as an extreme state of
 141 the terrestrial boundary layer. This is a result of two main differences: 1) The lower atmo-
 142 spheric density yields higher variability in the turbulent winds to carry a similar heat flux,
 143 and thus leading to stronger pressure bursts as detected by the InSight lander (Banfield et
 144 al., 2020), which result in greater intermittency in the turbulence. 2) The Martian surface
 145 exhibits much stronger temperature swings compared to the surface of Earth as a result of
 146 lower thermal inertia. This leads to a higher level of turbulent mixing in the boundary layer
 147 during daytime conditions compared to Earth's PBL (Temel et al., 2021) and much stronger
 148 stable stratification during nighttime conditions (Petrosyan et al., 2011). Kolmogorov's the-
 149 ory of turbulence is proposed based on the assumption of isotropic turbulence, which falls
 150 from reality also for the case of Earth's PBL. The Martian PBL, being an extreme counter-
 151 part of the terrestrial PBL, is not likely to be explained by a theory grounded on isotropic
 152 turbulence.

153 In Fig. 1, we investigate the pressure spectra for different local times, the size of tur-
 154 bulent structures vary with diurnal radiative forcing. We formulated our spectral analysis
 155 based on frequency. Therefore, large-scale eddies, driven by the large-scale turbulent mixing
 156 in the PBL, fall to the lower frequency bands, through the production range; whereas the
 157 smaller eddies are represented in the right side of the spectra within the inertial sub-range.
 158 The higher the frequency, the higher is the effect of dissipation on the turbulence spectra.
 159 The inertial sub-range refers to the range that the turbulence production conveys through
 160 the small and dissipative scales, in which the contribution of intermediate scales occurs.
 161 After the inertial range, the dissipative range lies. The typical time-scale for the dissipation
 162 range can be calculated as $(\nu/\epsilon)^{0.5}$, where ν is the kinematic viscosity and ϵ is the dissipa-
 163 tion rate of turbulence kinetic energy. Using the published values of ϵ (Temel et al., 2021),
 164 this time scale is around 0.2 s. Therefore, the present spectral range (0.001 Hz and 0.8 Hz)
 165 does not cover the dissipative range. Nevertheless, our resolution allows us to understand
 166 how fast the energy is transferred to the dissipative range by investigating the spectral slope
 167 within the inertial range.

168 We observe a slower energy transfer for the daytime conditions, represented with a slope
 169 of $\eta = [-1.5, -1.7] \sim -5/3$, in comparison to the proposed slope of Kolmogorov's theory,

170 $-7/3=-2.33$. Such a difference between the Kolmogorov's slope and the current observations
 171 and predictions, reveal that the contribution of intermediate scales are different for the
 172 case of the Martian PBL. This is as a result of much larger turbulent structures observed
 173 in the Martian daytime PBL. The dissipation rate of turbulence is inversely proportional
 174 to the turbulent length scale (Nakanishi & Niino, 2009; Angevine et al., 2010; Senel et al.,
 175 2019). Therefore, a higher amount of energy can be transferred to the edge of the dissipative
 176 range. In other words, the decay of energy in the inertial subrange through the dissipative
 177 range becomes softer with respect to the slope of Kolmogorov's theory, leading to a slower
 178 transition slope as shown both by the observations.

179 Despite the much smaller flow structures during the evening and night-time conditions,
 180 the spectra exhibits a much slower energy transfer in comparison to daytime conditions.
 181 Such that the spectra has a slope of $\eta = -1$, following the dimensional analysis of Tchen
 182 (1954) on boundary-layer turbulence that gives -1 scaling in sheared flow. It is likely to be
 183 a result of intermittency. Due to intermittent turbulence, the nocturnal flow regime exhibits
 184 lower and sporadic turbulent mixing, thus weaker energy content, in which the turbulent
 185 energy is transferred slower within the inertial sub-range. Another possible underlying mech-
 186 anisms for a slower energy transfer can be linked to Kelvin Helmholtz instabilities (Waite,
 187 2011; Iida & Nagano, 2007), which might also exist in planetary atmospheres (Johnson et
 188 al., 2014).

189 **4 The effect of a regional dust storm**

190 Fig. 2 presents the time evolution of the turbulence energy cascade as observed by the
 191 InSight lander. In our spectral analysis, sol 18, 46 and 55 correspond to the observational
 192 time periods before, during its onset and the maxima of dust storm (see Fig. 1c of Banfield
 193 et al. (2020)). For these sols, we used a sampling frequency of 2 Hz, which corresponds to
 194 the continuous frequency of the InSight pressure dataset before and after the dust storm
 195 season. However, as presented in Fig. S2, a dataset with a higher sampling frequency, 10
 196 Hz, provides consistent results with the ones obtained using a lower sampling frequency.

197 Before the dust storm, the inertial subrange exhibits the previously-illustrated slopes
 198 of $\eta = -5/3$ (daytime turbulence) and $\eta = -1$ (nocturnal turbulence). During the onset of
 199 the dust storm, despite the same behaviour in the daytime energy spectra, evening spectra
 200 show an energy spike between the production and inertial ranges. Recent studies show
 201 that spatially-inhomogeneous distribution of dust can lead to higher levels of turbulence
 202 (Wu et al., 2021; Chatain et al., 2021), consistent with the present energy spike we observe
 203 during the onset of a dust storm. The observational studies using MSL/REMS data showed
 204 that during a regional dust storm, the vertical gradient of temperature decreases and leads
 205 to a weaker stability (Ordonez-Etxeberria et al., 2020). A recent study using the InSight
 206 lander's data show that this weaker stability, combining to low-level jets forming at night
 207 under dusty seasonal conditions, cause strong nighttime turbulence (Chatain et al., 2021).
 208 Therefore, another possible explanation of the energy spike found in the present paper might
 209 be the spectral trace of a low-level jet, inducing energy production between the production
 210 and inertial ranges. Such a energy spike is not observed for the daytime conditions because
 211 the observed energy is much higher during the daytime so that such an additional input
 212 is negligible for daytime conditions. However, we find that this additional energy input is
 213 then rapidly dissipated in the evening spectra. Finally, we find that the additional energy
 214 injection is also present during the maxima of the dust storm for the daytime spectra. It
 215 causes an energy spike in the production range of spectrum, showing that dust-induced
 216 turbulent structures may act as the driving phenomena for the evening atmospheric surface
 217 layer.

218 5 The effect of gravity wave activity

219 As shown in Fig. 2 in the upper production range of evening and nighttime spectra, we
 220 observe a rapid decay of energy at lower frequencies below ~ 0.005 Hz. This spectral decay
 221 might be probing the existence of atmospheric gravity waves (GWs) appearing through the
 222 evening and night at specific seasons at the InSight landing site, which were detected by
 223 making use of pressure and wind speed perturbations by impedance relation (see Methods-
 224 Gravity wave detection section in (Banfield et al., 2020)). occurs at the frequency range
 225 of several hundreds of seconds, exhibiting the typical timescales of gravity waves (Gossard,
 226 1962; Fritts & Alexander, 2003). The turbulent energy within the given frequency range
 227 decays rapidly with a spectral slope of $\eta \sim -3$, which agrees with the terrestrial gravity
 228 wave cascade (Weinstock, 1978). However, a likely deviation from such a "near-universal"
 229 $\eta \sim -3$ spectra (Fritts et al., 1988; Smith et al., 1987; Fritts, 1989) may appear in certain
 230 conditions, especially due to the background winds for the atmosphere of Earth (Eckermann,
 231 1995). Our results indicate that such departures from the "near-universal" $\eta \sim -3$ spectra
 232 could also be true for the Martian gravity waves. To illustrate, at the peak phase of the dust
 233 storm i.e. Sol46 (Fig. 2e), the evening turbulence tends to decay faster than the $\eta \sim -3$
 234 slope, cascading with the slope of $\eta \sim -4$. Such a tendency can be related to the strong
 235 background winds, thus intense shear instabilities, as a consequence of the peak dust storm
 236 activity at sol 46. However, this departure recovers back to $\eta \sim -3$ at sol 55 (during the local
 237 evening and night) when the dust storm terminates (Fig. 2h-i). The gravity-wave signatures
 238 in our spectral-analysis are also consistent with the observations by (Banfield et al., 2020),
 239 which reports that the first 150 sols after landing exhibit an intense gravity-wave activity
 240 covering the time period of GW signatures probed here (i.e. sol 18, 46 and 55 in Fig. 2).
 241 The other possible mechanism can be related to the difference between the energy content
 242 for daytime and nocturnal conditions. As presented in Fig. 2, the upper production range
 243 contains a similar range of energy for daytime and nocturnal conditions but the nocturnal
 244 spectra reveals a much lower energy content within the inertial sub-range consistent with
 245 the extreme diurnal atmospheric stability difference on Mars (Petrosyan et al., 2011).

246 In order to elaborate our analysis of the effect of gravity wave activity and conclude
 247 whether this strong spectral slope of -3 is either a result of gravity wave activity or a typical
 248 nocturnal turbulence signature for the Martian atmosphere, we investigate two types of
 249 gravity wave activity types as classified by (Banfield et al., 2020): 1) bores and solitary
 250 waves, where the pressure anomaly is denoted with a sudden strong peak in the variation
 251 of the evening pressure fluctuations, 2) regular gravity waves, where the amplitude of the
 252 pressure anomaly is weak but the fluctuations last for a much longer duration. By making
 253 use of the published catalog of atmospheric gravity waves as observed by the InSight lander
 254 (Banfield et al., 2020), we investigate the evening turbulence spectrum for 6 different sols
 255 and present in Fig. 3 (left panel - bores and solitary waves, right panel - gravity waves).
 256 For the sols without any type of gravity wave activity (sol 56, 82 and 152), we find that
 257 the upper production still contains the spectral slope of -3, which leads to the conclusion
 258 that the rapid decay mechanism, denoted with a slope of -3, is a result of the extreme
 259 daytime/nocturnal stability difference. However, we still observe important consequences
 260 of gravity wave activity on the spectral dynamics of the Martian atmospheric turbulence.
 261 For the case of a strong gravity wave activity, as in sol 124 and 135, the energy content
 262 in the upper-production range is amplified. Moreover, as in sol 65, this energy injection
 263 is even stronger for the case of solitary waves and bores, as a result of higher pressure
 264 fluctuations with respect to a regular gravity wave so that the turbulence spectra includes
 265 even a sharper decay mechanism than -3. This shows that the Martian nocturnal boundary
 266 layer may become more turbulent with the presence of a gravity wave activity.

267 6 Conclusions and possible implications

268 Here, we present a spectral analysis of the in-situ observations of the InSight lander.
 269 In terms of the inertial sub-range, we find that the daytime turbulence is governed with

270 a slope of $-5/3$, and, the nocturnal turbulence consists of a slope of -1 , instead of $-7/3$ as
 271 suggested by Kolmogorov's energy cascade. The reported distinct behaviour of daytime and
 272 nocturnal inertial sub-ranges is due to the extreme stability difference in the Martian near-
 273 surface meteorological conditions. For daytime conditions, the deviation from Kolmogorov's
 274 theory is caused by the highly anisotropic nature of the Martian turbulence thanks to the
 275 high levels of turbulence kinetic energy. For the nocturnal conditions, it is linked to the
 276 intermittency and eddy bursts during night-time as shown in the present results. This
 277 implies that for future studies of the daytime Martian PBL, the contribution of large-scale
 278 eddies to turbulent transport, such as non-local transport (Ghannam et al., 2017), should be
 279 investigated. Moreover, the presence of intermittent eddy bursts can lead to sudden changes
 280 in the variation of the vertical wind, which can have important implications for nocturnal
 281 dust sedimentation. This also invokes a need for high temporal resolution observational
 282 studies of the variation of dust opacity on the Martian near-surface.

283 Based on our investigation of the effect of a regional dust storm on the energy cascade,
 284 we conclude that during the onset of a dust storm, additional energy is injected at the
 285 boundary between the production and inertial ranges. Moreover, we find that this injection
 286 can lead to sudden energy bursts in the energy spectra during the climax of the dust storm.
 287 This shows that, during dust storms, the nocturnal Martian PBL can be more turbulent
 288 despite the extreme stable stratification. During nocturnal conditions, increased night-time
 289 turbulence is linked with higher shear production. For Earth's PBL, nocturnal BL with
 290 high shear production occurs with the formation of low-level jets (LLJ) (Banta et al., 2002).
 291 LLJs are reinforced as a result of the dust cycle on Mars (Joshi et al., 1997). LLJs have
 292 important consequences for the transport of water on Earth (Higgins et al., 1997). Dust
 293 storm induced LLJs on Mars can have important consequences for the transport of volatiles
 294 from the surface to the atmosphere. Similar to the effect of a regional dust storm, we
 295 find that gravity wave activity leads to enhanced turbulence. This gravity-wave induced
 296 turbulence could affect the diurnal variation and the vertical transport of water, which
 297 drives the formation of boundary layer clouds on Mars (Daerden et al., 2010).

298 Acknowledgments

299 This work was financially supported by grant 12ZZL20N (to OT) of the Research Foundation
 300 Flanders. CB was supported by the Belgian Science Policy Office (BELSPO) via Chicxulub
 301 BRAIN-be (Belgian Research Action through Interdisciplinary Networks) project. AS and
 302 NM thank CNES and ANR (ANR-19-CE31-0008-08) for their support. OK acknowledges
 303 the support of the BELSPO through the ESA/PRODEX Program. We acknowledge NASA,
 304 CNES, partner agencies and Institutions (UKSA, SSO, DLR, JPL, IPGP-CNRS, ETHZ,
 305 IC, MPS-MPG, ISAE) and the operators of JPL, SISMOC, MSDS, IRIS-DMC and PDS for
 306 providing SEED data. This paper is InSight Contribution Number 225

307 Open Research

308 The InSight observations are available at [https://atmos.nmsu.edu/data_and_services/
 309 atmospheres_data/INSIGHT/insight.html](https://atmos.nmsu.edu/data_and_services/atmospheres_data/INSIGHT/insight.html) .

310 References

- 311 Albertson, J. D., Katul, G. G., Parlange, M. B., & Eichinger, W. E. (1998). Spectral
 312 scaling of static pressure fluctuations in the atmospheric surface layer: The interaction
 313 between large and small scales. *Physics of Fluids*, *10*(7), 1725–1732.
- 314 Angevine, W. M., Jiang, H., & Mauritsen, T. (2010). Performance of an eddy diffusivity–
 315 mass flux scheme for shallow cumulus boundary layers. *Monthly Weather Review*,
 316 *138*(7), 2895–2912.
- 317 Banerdt, W. B., Smrekar, S. E., Banfield, D., Giardini, D., Golombek, M., Johnson, C. L.,

- 318 . . . others (2020). Initial results from the insight mission on mars. *Nature Geoscience*,
319 1–7.
- 320 Banfield, D., Rodriguez-Manfredi, J., Russell, C., Rowe, K., Leneman, D., Lai, H., . . . others
321 (2019). Insight auxiliary payload sensor suite (apss). *Space Science Reviews*, 215(1),
322 1–33.
- 323 Banfield, D., Spiga, A., Newman, C., Forget, F., Lemmon, M., Lorenz, R., . . . others (2020).
324 The atmosphere of mars as observed by insight. *Nature Geoscience*, 1–9.
- 325 Banta, R., Newsom, R., Lundquist, J., Pichugina, Y., Coulter, R., & Mahrt, L. (2002).
326 Nocturnal low-level jet characteristics over kansas during cases-99. *Boundary-Layer
327 Meteorology*, 105(2), 221–252.
- 328 Chamberlain, T., Cole, H., Dutton, R., Greene, G., & Tillman, J. (1976). Atmospheric
329 measurements on mars: The viking meteorology experiment. *Bulletin of the American
330 Meteorological Society*, 57(9), 1094–1105.
- 331 Chatain, A., Spiga, A., Banfield, D., Forget, F., & Murdoch, N. (2021). Seasonal variability
332 of the daytime and nighttime atmospheric turbulence experienced by insight on mars.
333 *Geophysical Research Letters*, 48(22), e2021GL095453.
- 334 Daerden, F., Whiteway, J., Davy, R., Verhoeven, C., Komguem, L., Dickinson, C., . . .
335 Larsen, N. (2010). Simulating observed boundary layer clouds on mars. *Geophysical
336 research letters*, 37(4).
- 337 Eckermann, S. D. (1995). Effect of background winds on vertical wavenumber spectra of
338 atmospheric gravity waves. *Journal of Geophysical Research: Atmospheres*, 100(D7),
339 14097–14112.
- 340 Fritts, D. C. (1989). A review of gravity wave saturation processes, effects, and variability
341 in the middle atmosphere. *pure and applied geophysics*, 130(2), 343–371.
- 342 Fritts, D. C., & Alexander, M. J. (2003). Gravity wave dynamics and effects in the middle
343 atmosphere. *Reviews of geophysics*, 41(1).
- 344 Fritts, D. C., Tsuda, T., Kato, S., Sato, T., & Fukao, S. (1988). Observational evidence of a
345 saturated gravity wave spectrum in the troposphere and lower stratosphere. *Journal
346 of Atmospheric Sciences*, 45(12), 1741–1759.
- 347 Ghannam, K., Duman, T., Salesky, S. T., Chamecki, M., & Katul, G. (2017). The non-
348 local character of turbulence asymmetry in the convective atmospheric boundary layer.
349 *Quarterly Journal of the Royal Meteorological Society*, 143(702), 494–507.
- 350 Gómez-Elvira, J., Armiens, C., Castañer, L., Domínguez, M., Genzer, M., Gómez, F., . . .
351 others (2012). Rems: The environmental sensor suite for the mars science laboratory
352 rover. *Space science reviews*, 170(1-4), 583–640.
- 353 Gossard, E. E. (1962). Vertical flux of energy into the lower ionosphere from internal gravity
354 waves generated in the troposphere. *Journal of Geophysical Research*, 67(2), 745–757.
- 355 Hess, S., Henry, R., Leovy, C. B., Ryan, J., & Tillman, J. E. (1977). Meteorological results
356 from the surface of mars: Viking 1 and 2. *Journal of Geophysical Research*, 82(28),
357 4559–4574.
- 358 Higgins, R., Yao, Y., Yarosh, E., Janowiak, J. E., & Mo, K. (1997). Influence of the
359 great plains low-level jet on summertime precipitation and moisture transport over
360 the central united states. *Journal of Climate*, 10(3), 481–507.
- 361 Holstein-Rathlou, C., Gunnlaugsson, H., Merrison, J., Bean, K., Cantor, B., Davis, J., . . .
362 others (2010). Winds at the phoenix landing site. *Journal of Geophysical Research:
363 Planets*, 115(E5).
- 364 Iida, O., & Nagano, Y. (2007). Effect of stable-density stratification on counter gradient
365 flux of a homogeneous shear flow. *International Journal of Heat and Mass Transfer*,
366 50(1-2), 335–347.
- 367 Johnson, J. R., Wing, S., & Delamere, P. A. (2014). Kelvin helmholtz instability in planetary
368 magnetospheres. *Space Science Reviews*, 184(1-4), 1–31.
- 369 Joshi, M. M., Haberle, R. M., Barnes, J. R., Murphy, J. R., & Schaeffer, J. (1997). Low-
370 level jets in the NASA Ames Mars general circulation model. *Journal of Geophysical
371 Research Planets*, 102, 6511-6524. doi: 10.1029/96JE03765
- 372 Kaimal, J., Wyngaard, J., Haugen, D., Coté, O., Izumi, Y., Caughey, S., & Readings,

- 373 C. (1976). Turbulence structure in the convective boundary layer. *Journal of the*
374 *Atmospheric Sciences*, *33*(11), 2152–2169.
- 375 Kunkel, G. J., & Marusic, I. (2006). Study of the near-wall-turbulent region of the high-
376 reynolds-number boundary layer using an atmospheric flow.
- 377 Martínez, G., Valero, F., & Vázquez, L. (2009). Characterization of the martian surface
378 layer. *Journal of the atmospheric sciences*, *66*(1), 187–198.
- 379 Mason, P., & Derbyshire, S. (1990). Large-eddy simulation of the stably-stratified atmo-
380 spheric boundary layer. *Boundary-layer meteorology*, *53*(1-2), 117–162.
- 381 Mayor, S. D. (2017). Observations of microscale internal gravity waves in very stable atmo-
382 spheric boundary layers over an orchard canopy. *Agricultural and Forest Meteorology*,
383 *244*, 136–150.
- 384 Montabone, L., Forget, F., Millour, E., Wilson, R., Lewis, S., Cantor, B., . . . others (2015).
385 Eight-year climatology of dust optical depth on mars. *Icarus*, *251*, 65–95.
- 386 Nakanishi, M., & Niino, H. (2009). Development of an improved turbulence closure model
387 for the atmospheric boundary layer. *Journal of the Meteorological Society of Japan*.
388 *Ser. II*, *87*(5), 895–912.
- 389 Ordonez-Etxeberria, I., Hueso, R., Sánchez-Lavega, A., & Vicente-Retortillo, Á. (2020).
390 Characterization of a local dust storm on mars with rems/msl measurements and
391 marci/mro images. *Icarus*, *338*, 113521.
- 392 Petrosyan, A., Galperin, B., Larsen, S. E., Lewis, S., Määttänen, A., Read, P., . . . others
393 (2011). The Martian atmospheric boundary layer. *Reviews of Geophysics*, *49*(3).
- 394 Schmidt, H., & Schumann, U. (1989). Coherent structure of the convective boundary layer
395 derived from large-eddy simulations. *Journal of Fluid Mechanics*, *200*, 511–562.
- 396 Schofield, J., Barnes, J. R., Crisp, D., Haberle, R. M., Larsen, S., Magalhaes, J., . . . Wilson,
397 G. (1997). The mars pathfinder atmospheric structure investigation/meteorology
398 (asi/met) experiment. *Science*, *278*(5344), 1752–1758.
- 399 Seiff, A., Tillman, J. E., Murphy, J. R., Schofield, J. T., Crisp, D., Barnes, J. R., . . . others
400 (1997). The atmosphere structure and meteorology instrument on the mars pathfinder
401 lander. *Journal of Geophysical Research: Planets*, *102*(E2), 4045–4056.
- 402 Senel, C. B., Temel, O., Lee, C., Newman, C. E., Mischna, M. A., Muñoz-Esparza, D., . . .
403 Karatekin, O. (2021). Interannual, seasonal and regional variations in the martian
404 convective boundary layer derived from GCM simulations with a semi-interactive dust
405 transport model. *Journal of Geophysical Research: Planets*, *126*(10), e2021JE006965.
- 406 Senel, C. B., Temel, O., Muñoz-Esparza, D., Parente, A., & van Beeck, J. (2020). Gray
407 zone partitioning functions and parameterization of turbulence fluxes in the convective
408 atmospheric boundary layer. *Journal of Geophysical Research: Atmospheres*, *125*(22),
409 e2020JD033581.
- 410 Senel, C. B., Temel, O., Porchetta, S., Muñoz-Esparza, D., & van Beeck, J. (2019). A
411 new planetary boundary layer scheme based on les: Application to the xpia campaign.
412 *Journal of Advances in Modeling Earth Systems*, *11*(8), 2655–2679.
- 413 Smith, S. A., Fritts, D. C., & Vanzandt, T. E. (1987). Evidence for a saturated spectrum
414 of atmospheric gravity waves. *Journal of Atmospheric Sciences*, *44*(10), 1404–1410.
- 415 Spiga, A., Banfield, D., Teanby, N. A., Forget, F., Lucas, A., Kenda, B., . . . others (2018).
416 Atmospheric science with insight. *Space Science Reviews*, *214*(7), 1–64.
- 417 Spiga, A., Barth, E., Gu, Z., Hoffmann, F., Ito, J., Jemmett-Smith, B., . . . others (2016).
418 Large-eddy simulations of dust devils and convective vortices. *Space Science Reviews*,
419 *203*(1-4), 245–275.
- 420 Spiga, A., Forget, F., Lewis, S., & Hinson, D. (2010). Structure and dynamics of the con-
421 vective boundary layer on mars as inferred from large-eddy simulations and remote-
422 sensing measurements. *Quarterly Journal of the Royal Meteorological Society: A*
423 *journal of the atmospheric sciences, applied meteorology and physical oceanography*,
424 *136*(647), 414–428.
- 425 Spiga, A., Murdoch, N., Lorenz, R., Forget, F., Newman, C., Rodriguez, S., . . . others
426 (2020). A study of daytime convective vortices and turbulence in the martian planetary
427 boundary layer based on half-a-year of insight atmospheric measurements and large-

- 428 eddy simulations. *Journal of Geophysical Research: Planets*, e2020JE006511.
- 429 Taylor, P. A., Catling, D. C., Daly, M., Dickinson, C. S., Gunnlaugsson, H. P., Harri, A.-
430 M., & Lange, C. F. (2008). Temperature, pressure, and wind instrumentation in the
431 phoenix meteorological package. *Journal of Geophysical Research: Planets*, 113(E3).
- 432 Tchen, C.-M. (1954). Transport processes as foundations of the heisenberg and obukhoff
433 theories of turbulence. *Physical Review*, 93(1), 4.
- 434 Temel, O., Senel, C. B., Porchetta, S., Muñoz-Esparza, D., Mischna, M. A., Van Hoolst, T.,
435 ... Karatekin, Ö. (2021). Large eddy simulations of the martian convective bound-
436 ary layer: towards developing a new planetary boundary layer scheme. *Atmospheric*
437 *Research*, 250, 105381.
- 438 Toigo, A. D., Richardson, M. I., Ewald, S. P., & Gierasch, P. J. (2003). Numerical simulation
439 of martian dust devils. *Journal of Geophysical Research: Planets*, 108(E6).
- 440 Tsuji, Y., Fransson, J. H., Alfredsson, P. H., & Johansson, A. V. (2007). Pressure statistics
441 and their scaling in high-reynolds-number turbulent boundary layers. *Journal of Fluid*
442 *Mechanics*, 585, 1.
- 443 Tsuji, Y., & Ishihara, T. (2003). Similarity scaling of pressure fluctuation in turbulence.
444 *Physical Review E*, 68(2), 026309.
- 445 Viúdez-Moreiras, D., Gómez-Elvira, J., Newman, C., Navarro, S., Marin, M., Torres, J., ...
446 others (2019). Gale surface wind characterization based on the mars science laboratory
447 rema dataset. part i: Wind retrieval and gale's wind speeds and directions. *Icarus*,
448 319, 909–925.
- 449 Waite, M. L. (2011). Stratified turbulence at the buoyancy scale. *Physics of Fluids*, 23(6),
450 066602.
- 451 Weinstock, J. (1978). On the theory of turbulence in the buoyancy subrange of stably
452 stratified flows. *Journal of the atmospheric sciences*, 35(4), 634–649.
- 453 Wu, Z., Richardson, M. I., Zhang, X., Cui, J., Heavens, N. G., Lee, C., ... others (2021).
454 Large eddy simulations of the dusty martian convective boundary layer with marswrf.
455 *Journal of Geophysical Research: Planets*, 126(9), e2020JE006752.

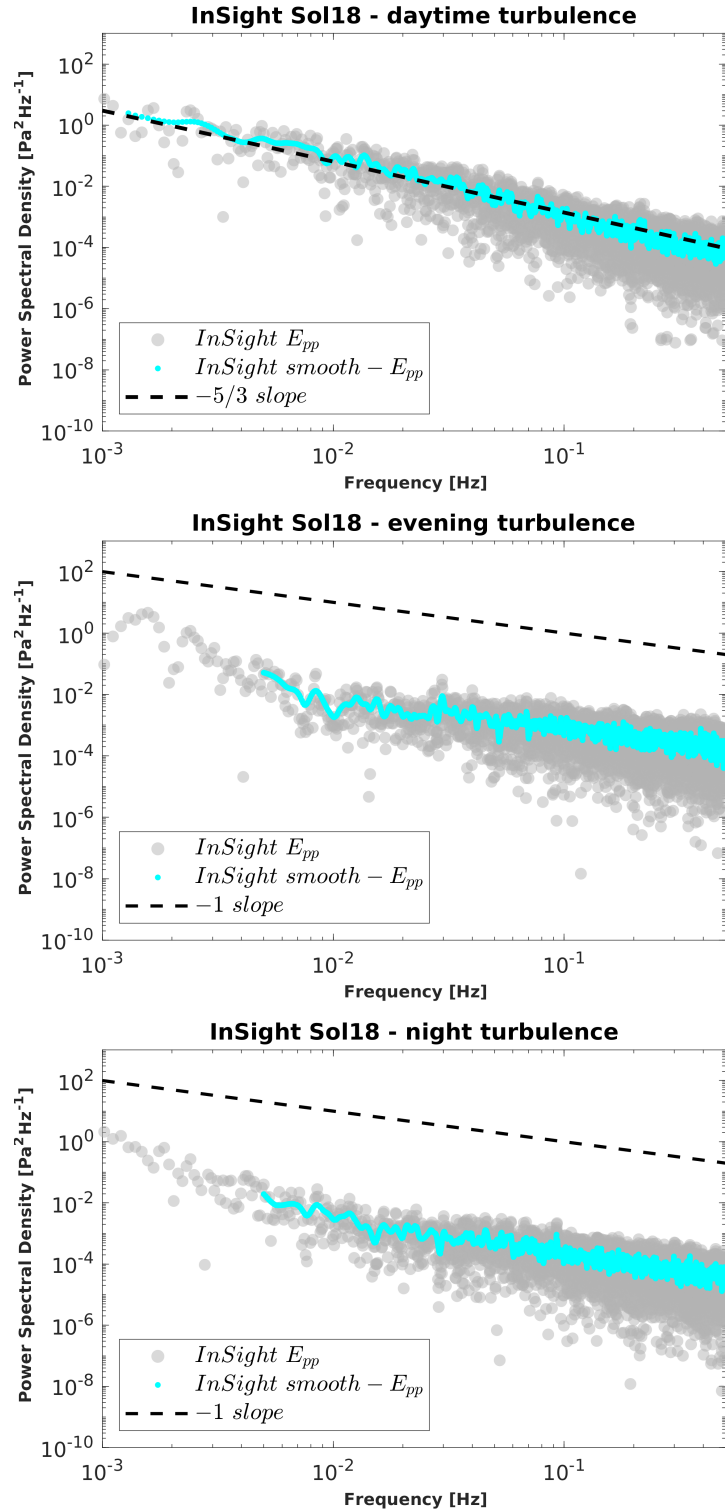


Figure 1. Turbulence spectra obtained by the InSight observations for different local times. The results are normalized with the maximum energy at the lowest frequency: (a) - observations for daytime conditions, (b) - observations for evening conditions, (c) - observations for nocturnal conditions.

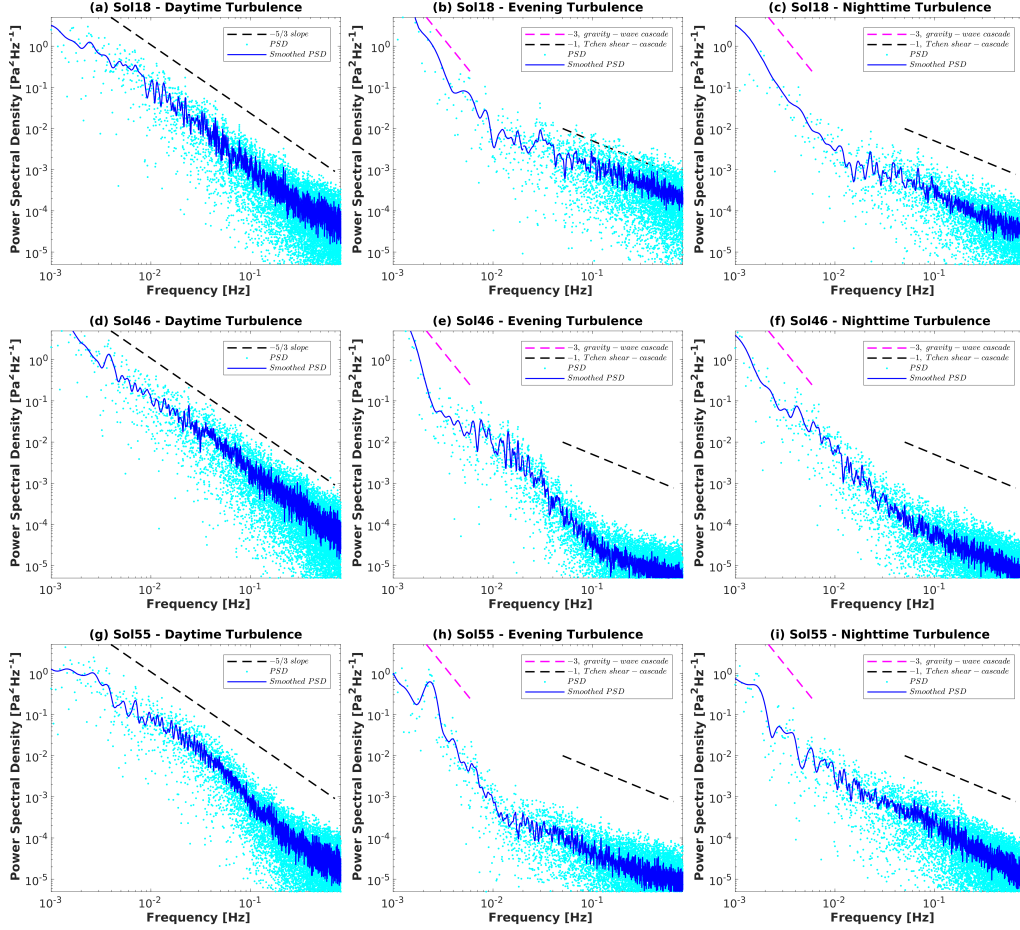


Figure 2. Turbulence spectra acquired by the InSight Observations before (sol 18, $L_s = 306^\circ$), during the onset (sol 46, $L_s = 323^\circ$), at the climax of the dust storm (sol 55, $L_s = 328^\circ$). Sols are chosen based on the variation of dust opacity by the InSight lander (Banfield et al., 2020).

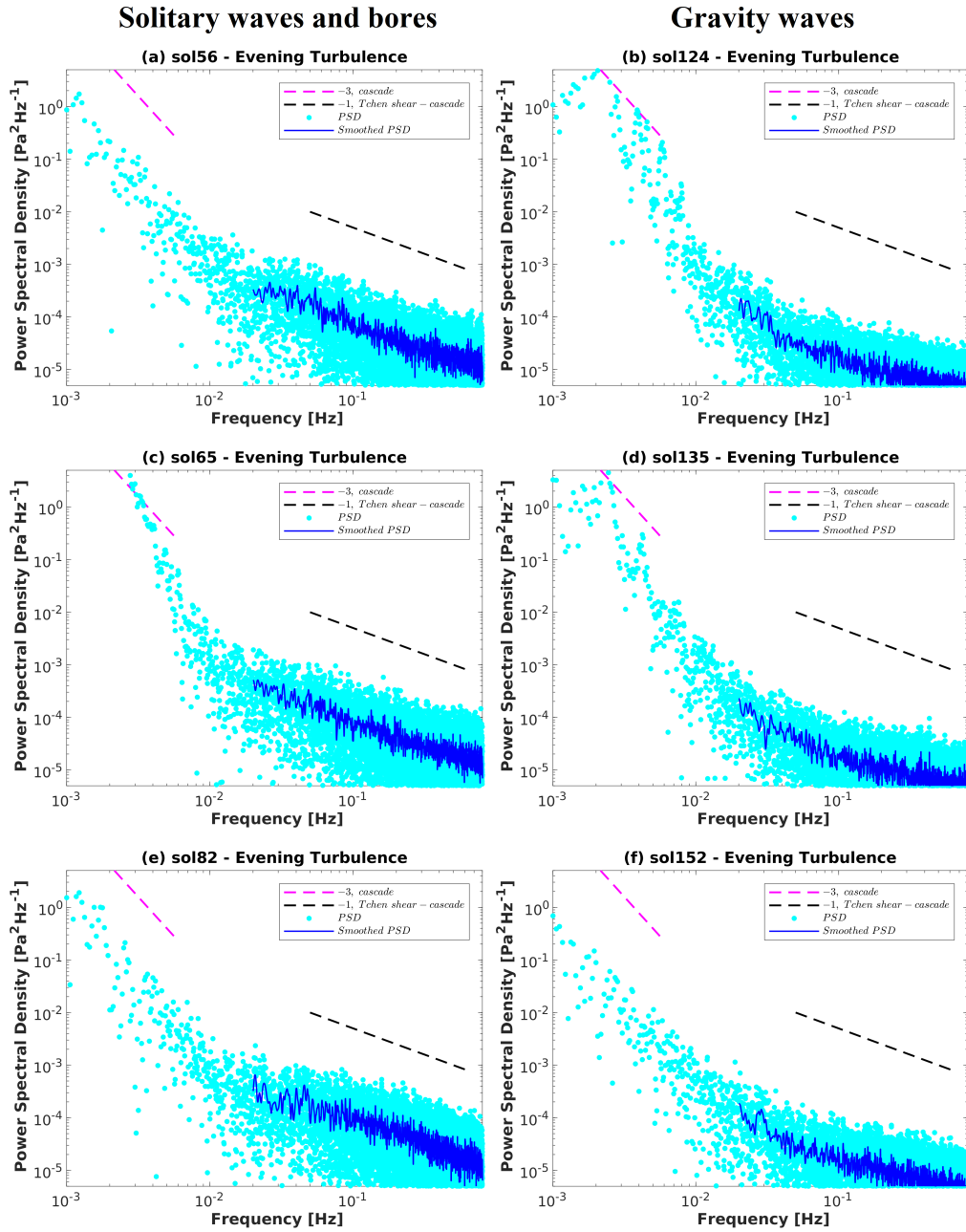


Figure 3. Turbulence spectra acquired for the days with and without solitary waves and bores (left panel, sol 65 with solitary wave and bores), and gravity waves (right panel, sol 124 and 135 with gravity waves). The sols are selected according to the gravity wave activity catalog acquired based on the InSight lander’s pressure observations (Banfield et al., 2020).